

# Entropic attraction condenses like-charged interfaces composed of self-assembled molecules

Ariel Steiner<sup>||</sup>, Pablo Szekely<sup>||,†</sup>, Or Szekely<sup>||</sup>, Tom Dvir<sup>||,†</sup>, Roi Asor<sup>||</sup>, Naomi Yuval-Naeh<sup>‡</sup>, Nir Keren<sup>‡</sup>, Ellina Kesselman<sup>§</sup>, Dganit Danino<sup>§,¶</sup>, Roy Resh<sup>||,†</sup>, Avi Ginsburg<sup>||</sup>, Vicky Guralnik<sup>||</sup>, Esther Feldblum<sup>||</sup>, Carmen Tamburu<sup>||</sup>, Menachem Peres<sup>||</sup> and Uri Raviv<sup>||,\*</sup>

<sup>||</sup> The Institute of Chemistry, <sup>†</sup> The Racah Institute of Physics, <sup>‡</sup>The Alexander Silverman Institute of Life Sciences, The Hebrew University of Jerusalem, Edmond J. Safra Campus, Givat Ram, 91904 Jerusalem, Israel. <sup>§</sup>Department of Biotechnology and Food Engineering, and <sup>¶</sup> The Russell Berrie Nanotechnology Institute, Technion - Israel Institute of Technology, Haifa, 32000 Israel.

\* To whom correspondence should be addressed. E-mail: [raviv@chem.ch.huji.ac.il](mailto:raviv@chem.ch.huji.ac.il).

## Supporting Information

### §1. Lipid properties

The physical properties of the lipids, used in this study, are defined and summarized in this section. The lipid volume fraction,  $\phi$ , is estimated by:

$$(S1) \quad \phi = V_{lipid} / V_{tot} = (v_L \cdot m_{lipid}) / (v_L \cdot m_{lipid} + V_{H_2O}).$$

$V_{lipid}$  is the total volume that the lipid occupies.  $V_{tot}$  is the total solution volume.  $m_{lipid}$  is the lipid mass,  $v_L$  is the lipid specific volume and  $V_{H_2O}$  is the water volume. Other lipid properties, taken from the literature or inferred from literature data, are summarized in Table S1.

**Table S1.** Properties of the lipids used in this study, based on literature data.

	DOPS	DOPC	DSPS	DLPS	DOTAP
Molecular weight, $M_w$ , (gr/mol)	810 <sup>1</sup>	786.1 <sup>1</sup>	814 <sup>1</sup>	645.7 <sup>1</sup>	698.5 <sup>1</sup>
Melting temperature, $T_m$ , (°C)	-11 <sup>2</sup>	-20 <sup>2</sup>	68 <sup>1</sup>	13 <sup>3</sup>	-8 <sup>4</sup>
Bending rigidity, $\kappa$ , ( $k_B T$ )	26 <sup>a</sup>	20 <sup>a</sup>	47 <sup>a</sup>	9 <sup>a</sup>	26 <sup>a</sup>
lipid specific volume, $v_L$ , (ml/gr)	0.913 <sup>5</sup>	0.998 <sup>5</sup>	0.9 <sup>b</sup>	0.854 <sup>b</sup>	0.879 <sup>6</sup>
Volume of the two tails, $V_C$ , (Å <sup>3</sup> )	984 <sup>c</sup>	984 <sup>c</sup>	972 <sup>d</sup> , 1023.2 <sup>n</sup>	672 <sup>e</sup>	984 <sup>c</sup>
Area per head-group, $A_h$ , (Å <sup>2</sup> )	64.1 <sup>c</sup>	72.5 <sup>c</sup>	40.8 <sup>c</sup>	55.2 <sup>e</sup>	65 <sup>4</sup>
tail thickness, $l_c$ , (Å)	15.4 <sup>c</sup>	13.6 <sup>c</sup>	24.2 <sup>f</sup>	10.4 <sup>e</sup>	15.4 <sup>c</sup>
Packing parameter <sup>2</sup> , $p$	0.997 <sup>c</sup>	0.998 <sup>c</sup>	0.983 <sup>d</sup> , 1.035 <sup>f</sup>	1.16 <sup>e</sup>	0.983
Head to-head membrane thickness, $\delta$ , (Å)	39 <sup>c</sup>	36.9 <sup>c</sup>	49.36 <sup>c</sup>	29.1 <sup>c</sup>	35 <sup>7</sup>

<sup>a</sup> Data from ref. 8, assuming  $\kappa \propto (l_c^2)$ , where  $l_c$  is the membrane tail thickness.<sup>8</sup>

<sup>b</sup>  $v_L = (N_A V_L)/M_w$ , where  $N_A$  is Avogadro's number,  $V_C$  is the volume of the two chains,  $V_L$  is the total lipid volume,  $V_L = V_C + V_H$ .  $V_H = 244 \text{ \AA}^3$ ,<sup>5</sup> is the head volume, assuming:  $V_{H, DOPS} = V_{H, DMPS} = V_{H, DLPS} = V_{H, DSPS}$ .

<sup>c</sup> Data from ref. 5, assuming  $A_h(\text{DSPS, gel}) = A_h(\text{DMPS, gel})$ , both in the gel phase,  $V_C(\text{DOTAP}) = V_C(\text{DOPS})$ ,  $l_c(\text{DOTAP}) = l_c(\text{DOPS})$ ,  $\delta(\text{DSPS}) = \delta(\text{DMPS}) + 4 \cdot 1.265 \text{ \AA}$  (the C-C bond length), and  $\delta(\text{DLPS, fluid}) = 2 \cdot \{l_H(\text{PS, fluid}) + l_c(\text{DLPC, fluid})\}$ , where  $l_H$  is the head thickness and is  $l_H = 0.5 \cdot (\delta - 2 \cdot l_c)$  and  $l_c(\text{DLPC, fluid}) = l_c(\text{DLPS, fluid})$ .

<sup>d</sup> Data from ref. 9, assuming  $V_C(\text{DSPS, gel}) = V_C(\text{DSPC, gel})$ .

<sup>e</sup> Data from ref. 10, assuming  $l_c(\text{DLPS}) = l_c(\text{DLPC})$ ,  $A_h(\text{DLPS, liquid}) = A_h(\text{DLPC, fluid}) - 8 \text{ \AA}^2$  and  $V_C(\text{DLPS}) = V_C(\text{DLPC})$ .

<sup>f</sup> Data from ref. 11, using the maximum tail length  $l_{\text{max}} = (1.54 + 1.26 \cdot n) \text{ \AA}$  and volume  $V_C = 2 \cdot (27.4 + 26.9 \cdot n) \text{ \AA}^3$ , where  $n$  is the number of alkyl chain carbon atoms.

## **§2. Deviations from theory of DOPS in water**

Figure S1A presents the data in Figure 2 in an alternative way. The figure directly compares the values of the lamellar repeat spacing,  $D$ , with the ideal-swelling separation,  $D_{\text{ideal}}$ , given by eq. 2.

In the derivation of the Poisson-Boltzmann (PB) equation (eq. 8) it is assumed that the ionic charge distributions are smeared out and are represented as smoothly varying functions. The PB theory is a mean-field theory and neglects fluctuations and correlations<sup>12</sup>. In the case of no added salt (i.e. only counterions are present) when taking into account the layer-charge and counterions fluctuations,<sup>13</sup> there is a reduction of the electrostatic repulsive pressure in the Gouy Chapman region (eq. 8)

$$(S2) \quad P_{\text{elec}} \approx \frac{\pi k_B T}{2l d_w^2} - \frac{k_B T}{d_w^3},$$

where  $l$  is the Bjerrum length (eq. 9) and  $d_w$  is the water spacing between bilayers.

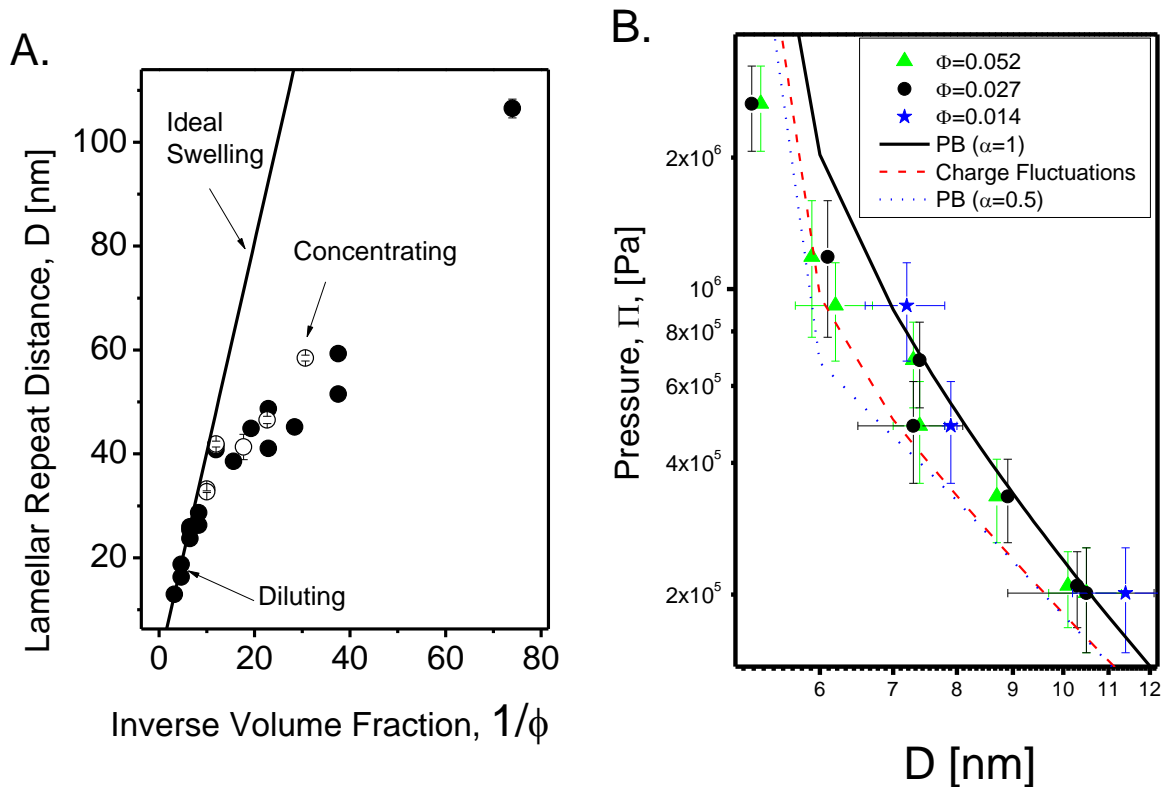
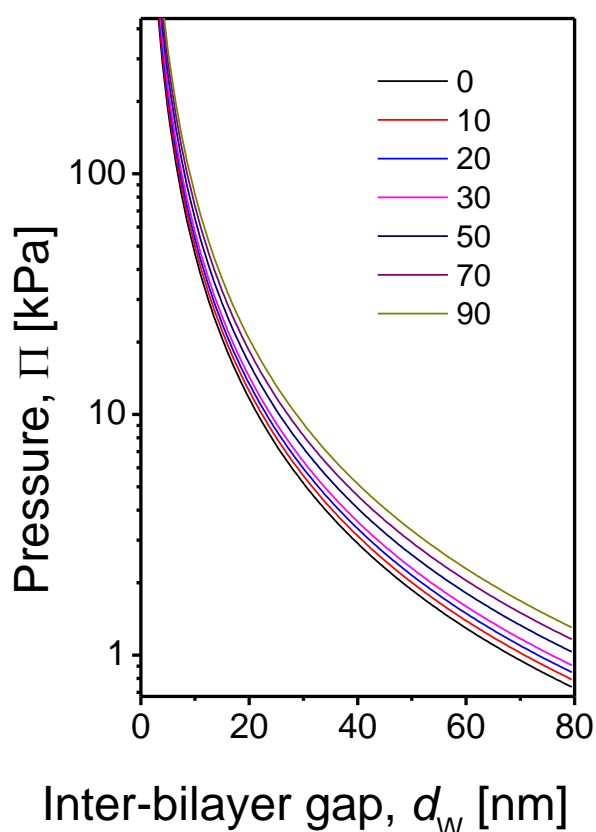


Figure S1. **A.** Swelling behavior of DOPS in pure water. The lamellar repeat distance,  $D$ , obtained from small angle x-ray scattering (SAXS) measurements, is plotted vs. the inverse DOPS volume fraction,  $1/\phi$  ( $\phi$  is calculated using Eq. S1). The solid line corresponds to the ideal-swelling distance given by  $D_{\text{ideal}} = \delta/\phi$  (eq. 2), where  $\delta = 4.04 \pm 0.02$  nm is the bilayer thickness.  $\delta$  was obtained from a fit of the ideal-swelling relation to the high volume fraction measurements and based on form-factor analysis of dilute DOPS solutions. **B.** Osmotic pressure,  $\Pi$ , as a function of  $D$  for different DOPS volume fractions in pure water, as indicated. The data of Figure 4 are plotted on an expanded scale at the range of high osmotic stress. The black solid line is the theoretical pressure (Eq. 12, using the PB solution in the Gouy Chapman region with  $\alpha=1$ ), as in Figure 4. The dashed red curve is similar to the solid curve but with electrostatic repulsion that takes into account the layer-charge fluctuation and the counterions fluctuations (eq. S2). The dotted blue line is similar to the solid curve but with electrostatic repulsion that assumes that only half of the counterions are dissociated,  $\alpha=0.5$  (eq. 8). At lower pressures the broken curves overlap with the solid curve.

### §3. The interactions between charged membranes at different temperatures

Figure S2 shows the theoretical pressure,  $\Pi$ , between charged membranes (eq. 12) as a function of the water spacing between them,  $d_w$ , at several temperatures. As expected, the total repulsion between charged interfaces increases with temperature.



**Figure S2.** The estimated total pressure,  $\Pi$ , between charged interfaces (using eq. 12 and the parameters relevant for DLPS provided in Table S1), as a function of the inter-bilayer gap,  $d_w$ , at different temperatures (in °C), as indicated in the figure.

#### **§4. Microscopy images**

We support our X-ray data with complementary electron and light microscopy data showing that samples that deviated from ideal-swelling behavior micro-phase separated into a lamellar phase and a disordered lipid phase. Cryogenic-transmission electron microscopy (cryo-TEM) images (Figure S3) show mainly the disordered phase. Cryo-TEM examines objects that are dispersed within the thin vitrified sample layer (50 – 200 nm) formed on the supporting grid. The images show real space information about the shape of individual objects in the disordered phase that solution X-ray scattering does not provide. Light microscopy images (Figure S4) look at a much larger length scale, which are not accessible to the X-ray scattering experiments or electron microscopy, and show that the overall dimensions of the lamellar phase is tens to thousands of microns and increases with the concentration of lipid.

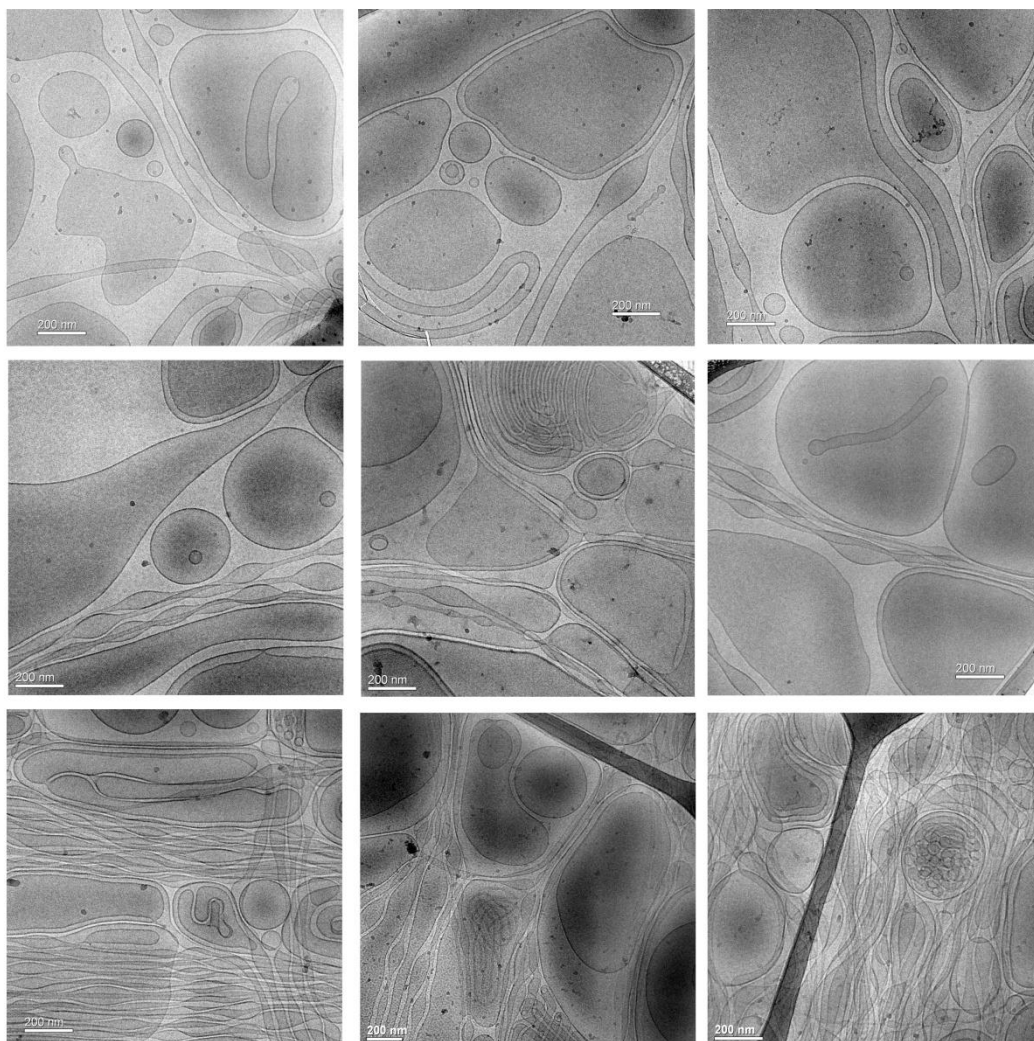


**Figure S3.** Cryogenic transmission electron microscopy images of DOPS at  $\phi=0.014$  showing uni-lamellar vesicles and multi-lamellar vesicles (MLVs) of various shapes including closed tubular and multi tubular structures.

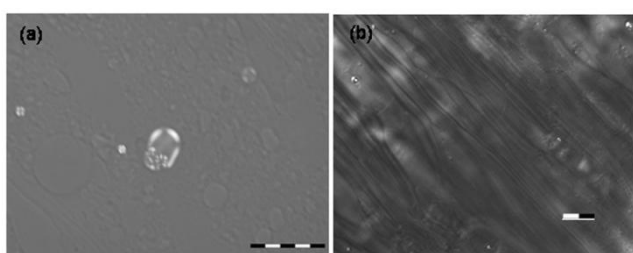


**Figure S4.** Light microscopy (LM) images of high and low concentrations of DOPS. **(a)** Polarized LM of DOPS at  $\Phi=0.084$ ; scale bar = 50  $\mu\text{m}$ . The bright white crosses are the hallmark of a lamellar phases composed of large multi lamellar vesicles (MLVs). The other features in the figure suggest that this phase coexists with smaller vesicles in a disordered phase. **(b)** Differential interference contrast (DIC) image of DOPS at  $\Phi=0.215$ ; scale bar = 15  $\mu\text{m}$ . The straight lines fill the entire image, indicating that the lipids are in a single lamellar ( $L_\alpha$ ) phase.

## §5. Effect of temperature

Here we provide additional support to Figure 5 and confirm that DOPS exhibits a similar temperature response to that of DLPS. Figure S5 shows the reduction in the lamellar repeat

distance,  $D$ , normalized to the temperature-dependent ideal-swelling distance,  $D_{\text{ideal}}(T) = \delta(T)/\phi$ . We used the temperature variation of the membrane thickness  $\delta(T)$ , obtained from the form-factor analysis (shown at the inset to Figure S5), to calculate  $D_{\text{ideal}}$  at each temperature. As in the case of DLPS, lower lipid concentrations deviate more than higher concentrations.

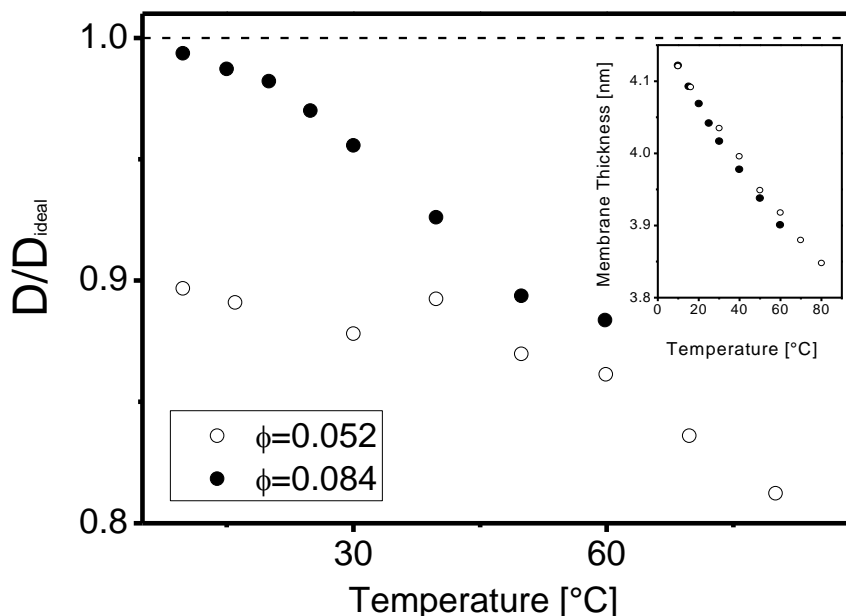


**Figure S5.** The temperature dependence of the ratio between the lamellar repeat distance,  $D$ , and the ideal-swelling distance,  $D_{\text{ideal}}$ , of DOPS. The lipid volume fraction,  $\phi$ , is indicated in the figure. The inset shows the variation of the DOPS membrane thickness with temperature, obtained from the analysis of the X-ray scattering form-factor. We used those membrane thicknesses to calculate  $D_{\text{ideal}}$  at each temperature.

### **§6. Effect of added salt**

Here we show additional data that support our conclusion that the behavior is essentially similar in the presence of monovalent salt. We present the osmotic stress curves of DOPS in the presence of low salt concentrations (Figure S6A) and the behavior of DLPS at different salt concentrations (Figure S6B). In both graphs we compare the data with theory. Finally, we compare the water spacing,  $d_w$ , of DOPS and DLPS at different salt concentrations (Figure S6C) and find that the two lipids follow a similar curve.

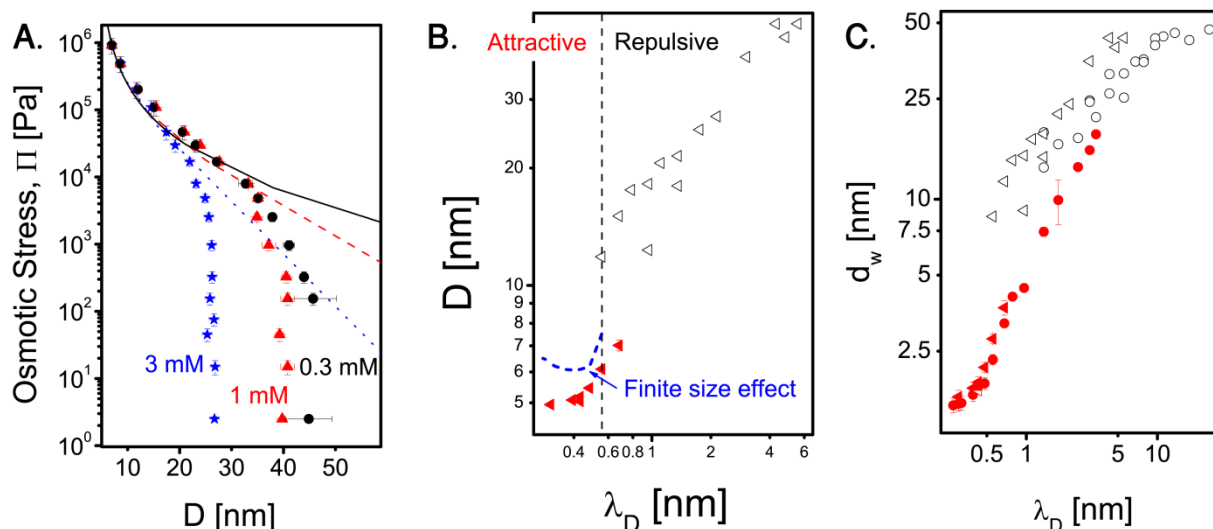


**Figure S6.** Effect of added salt on D. **A.** The osmotic stress,  $\Pi$ , as a function of D for DOPS at different NaCl concentrations. Solid circles, triangles, and stars are DOPS at 0.3, 1 and 3 mM NaCl solutions, respectively. The solid, dashed and dotted curves are the corresponding theoretical pressures calculated using eq. 12 with the Poisson-Boltzmann (PB) electrostatic repulsion energy (eq. 8). **B.** DLPS lamellar repeat distance, D, as a function of the Debye-Hückel screening length,  $\lambda_D$  (eq. 11). NaCl solutions were added to lyophilized DLPS powder to obtain DLPS volume fractions,  $\phi$ , of 0.014. The blue broken curve is the locus of calculated distances (at each salt concentration) for which the total interaction energy between the charged membranes (eq. 3) reached its minimum. The electrostatic repulsion energy term is the reduced PB theory, corrected for discrete solvent effects (eq. 13). The vertical dotted line at  $\lambda_D \approx 0.55$  nm (corresponding to ca. 300 mM NaCl) indicates the largest  $\lambda_D$ , above which the discrete theory predicts a net repulsive interaction. As in Figure 6, solid symbols correspond to the measured DLPS repeat distances, originally observed at high salt concentrations where the predicted net interaction energy is attractive. Open symbols correspond to the measured DLPS repeat distances, originally observed at low salt concentrations, where the predicted interaction energy is repulsive. **C.** Comparison of DLPS with DOPS. The water gap,  $d_w$ , as a function of  $\lambda_D$ , where  $d_w = D - \delta$  and  $\delta$  is the corresponding thickness of each bilayer (see Table S1). Symbols are as in (B.) for DLPS and as in Figure 6 for DOPS (open and solid circles).

## §7. Neutral membranes in the presence of multivalent ions

Here we demonstrate that dipolar (neutral) interfaces behave as charged membranes in the presence of multivalent ions. Sodium ( $\text{Na}^+$ ), magnesium ( $\text{Mg}^{2+}$ ), zinc ( $\text{Zn}^{2+}$ ), and calcium ( $\text{Ca}^{2+}$ ) ions are crucial for the regulation and function of many membrane-associated processes. While these ions are expected to bind or remain close to charged interfaces, there is a great deal of curiosity about what these ubiquitously mobile ions do near or at zwitterionic interfaces. Therefore, we studied the adsorption of  $\text{Ca}^{2+}$  onto neutral (zwitterionic) membranes composed of lipid with phosphatidylcholine (PC) head-groups. Specifically, we looked at 1,2-dilauroyl-sn-glycero-3-phosphocholine (DLPC), purchased from Avanti Polar Lipids, Inc. (Alabaster, AL, USA).

Using solution X-ray scattering<sup>14</sup> the repeat lamellar distance,  $D$ , was measured and plotted as a function of  $\text{CaCl}_2$  concentration in Figure S7. Unlike charged membranes, in pure water the neutral (zwitterionic) membranes do not have electrostatic repulsive interactions. The interaction between them is a balance between short-ranged hydration repulsion, undulation repulsion, and van der Waals (vdW) attraction, which leads to a small bilayer separation of  $d_w < 3$  nm.

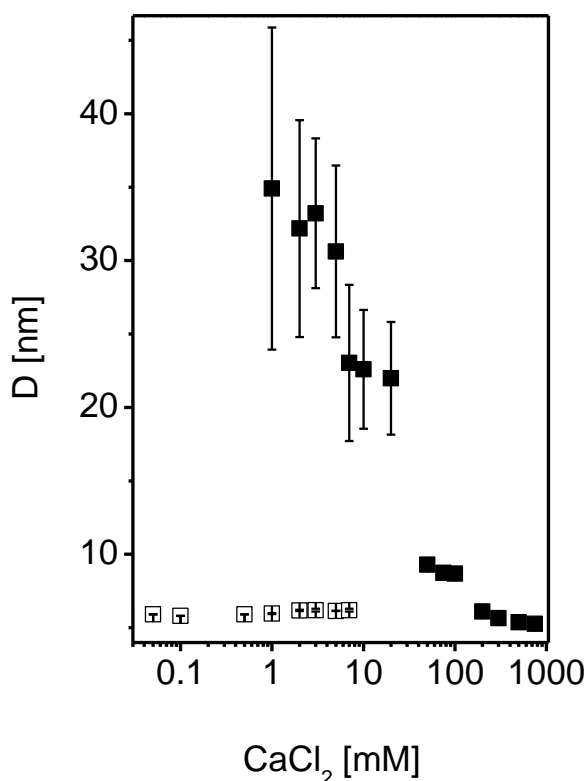


**Figure S7.** The lamellar repeat distances,  $D$ , of DLPC as a function of  $\text{CaCl}_2$  concentration. The lipid volume fraction,  $\phi$ , was ca. 0.014. Open symbols correspond to membranes that did not adsorb calcium ions, whereas solid symbols correspond to membranes that adsorbed the ions. When two phases coexist, the phase shown with solid symbols was the dominating one. The error bars (shown unless they are smaller than the symbols) correspond to statistical errors of repeated measurements.

For low  $\text{CaCl}_2$  concentrations, only one phase exists (open symbols in Figure S7), with  $d_w < 3$  nm, as in pure water. At salt concentrations of 1 mM, a second phase appears, in which the membranes swell to a large lamellar spacing (solid symbols in Figure S7). This is the equilibrium phase.<sup>15-17</sup> After equilibrium is reached (generally between a week to two months after preparation), most of the lipids are in the primary phase, indicated by the solid symbols in Figure S7, and exhibit large inter-lamellar spacings when the  $\text{Ca}^{2+}$  concentration reaches ca. 1

mM. This spacing is similar to the spacing measured for charged membranes composed of DLPS or DOPS in a 3 mM NaCl salt solution that has a similar ionic strength (Figure S6C).

We attribute the large spacing to the charging of the zwitterionic membrane, resulting from the adsorption of the divalent cation onto the PC head-groups and leading to electrostatic repulsion between the membranes. At higher salt concentrations, while more  $\text{Ca}^{2+}$  ions may adsorb onto the bilayers, the electrostatic repulsion is also screened by the presence of more ions in the solution and the lamellar repeat spacing decreases. The latter behavior is in accordance with earlier findings<sup>18</sup> on phosphatidylcholines at higher lipid concentrations (30 wt%).

In the earlier study,<sup>18</sup> however, the  $\text{Ca}^{2+}$  ions adsorbed onto the lipids, charged the membranes and led to their ideal-swelling, according to  $D_{\text{ideal}} = \delta/\phi$ , where  $\delta$  is the membrane thickness and  $\phi$  is the lipid volume fraction. As we showed in Figure S1, this behavior is typical for charged membranes at lipid concentrations above ca. 15 wt%. In our lipid volume fraction (ca. 0.014) we obtained  $D$  values that are significantly shorter than the ideal-swelling distance given by  $\delta/\phi$ . This result is consistent with our findings that self-assembled like-charged interfaces, composed of charged lipids (e.g. DOPS or DLPS), deviate markedly from ideal-swelling behavior below the aforementioned critical lipid concentration.

The results show that membranes composed of saturated zwitterionic lipids that adsorb divalent ions follow a similar behavior to that of membranes composed of charged lipids. This suggests that the adsorbed ions induce the formation of a disordered phase that coexists with the lamellar phase. The disordered phase is depleted by the lamellar phase and applies an osmotic stress to it. The lamellar spacing is determined by equating the water chemical potential and the pressures of the two phases. Other saturated PC lipids and other divalent and trivalent ions behave similarly.<sup>14</sup>

## **§8. Biomembranes**

Here we present solution X-ray scattering curves of living cells from four different kingdoms and membranes isolated from a plant or alga. These biomembranes exhibit correlation

distances that fall within the range of our much simpler synthetic bilayers' lamellar repeat distances.

Lipid membranes are fundamental structural elements of living cells. They form the external and internal boundaries of cells (plasma and organelles), provide the surface at which proteins and organic molecules are synthesized and processed (endoplasmic reticulum and Golgi apparatus) and in which energy is captured or consumed (chloroplasts and mitochondria). Biomembranes are complex and include membrane proteins and various lipids and are considered to operate outside of equilibrium.<sup>19</sup> Still they form self-assembled charged and rigid interfaces. Earlier microscopy studies suggest that biomembranes in cells do not swell ideally as our self-assembled pure charged lipid rigid interfaces do.<sup>19</sup>

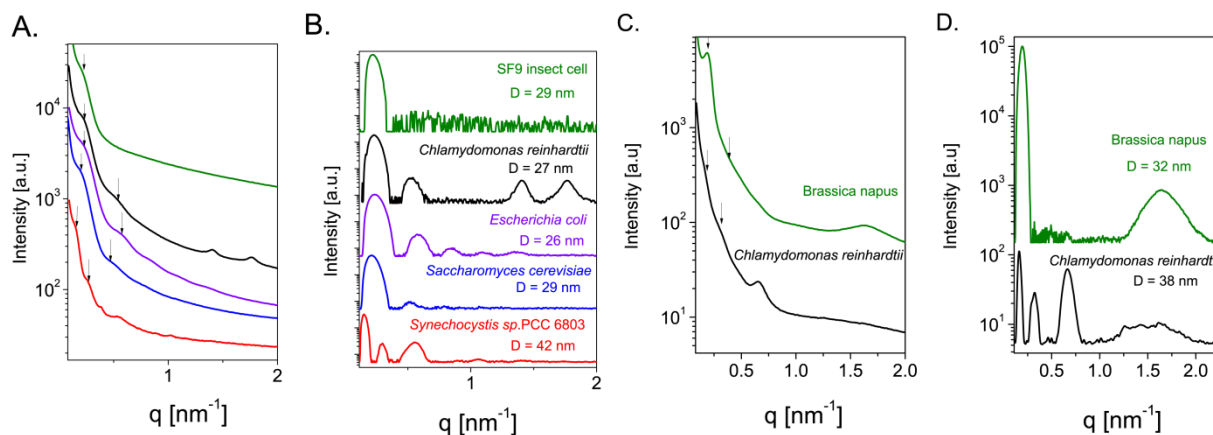


**Figure S8.** Radially integrated solution small angle X-ray scattering curves from different cells and isolated biomembranes. **A.** Raw data from cells grown as described.<sup>20-23</sup> **B.** The scattering curves shown in (A.) after baseline subtraction. **C.** Raw data of radially integrated scattering curves from membranes that were isolated from *Chlamydomonas reinhardtii* and *Brassica napus* as described.<sup>24</sup> **D.** The scattering curves shown in (C.) after baseline subtraction. The arrows in (A.) and (C.) indicate the principle and second harmonic scattering lamellar peaks and their corresponding repeat distances, D, are given in (B.) and (D.) The intensity is given in arbitrary units and the curves are shifted only for clarity of presentation. The origin of the other peaks is unclear at this stage.

To explore the structure of biomembranes we measured five species of prokaryotic and eukaryotic organisms representing four taxonomical kingdoms (Bacteria, Fungi, Plantae and Animalia). Measurements were performed *in vivo* on samples compacted to the bottom of capillary tubes by centrifugation at relative centrifugal forces (RCF) of 6000 g.

As an example of the basic prokaryote cell type, the Gram-negative *Escherichia coli* was chosen. Gram-negative bacteria have two membrane systems, outer and plasma membranes. In

comparison, we studied the Gram-negative cyanobacterium *Synechocystis* sp. PCC 6803. In addition to the outer and plasma membranes cyanobacteria contain sacs of photosynthetic thylakoid membranes inside their cell.

The structure of eukaryotes is more complex than prokaryotes. As examples of eukaryotes tissue culture SF9 insect cells, unicellular yeast *Saccharomyces cerevisiae* and the photosynthetic green alga *Chlamydomonas reinhardtii* were measured. SF9 insect cells contain plasma, nuclear, endoplasmic reticulum, Golgi, peroxisome, and mitochondria charged membrane systems. Yeast and alga cells contain, in addition, a vacuolar membrane system. On top of that, alga cells have chloroplasts with their inner, outer, and thylakoid membrane systems. Figure S8A and B show the solution SAXS curves and the correlation distances observed in those cells. Those correlation distances most likely originate from the lamellar phases that membranes form in each cell type.

In addition, *in vitro* measurements of membranes isolated from *Chlamydomonas reinhardtii* and the vascular plant *Brassica napus* were performed (the membranes were isolated as described<sup>24</sup> and prepared for X-ray scattering measurement as the *in vivo* samples). The membrane composition of the plant cell is similar to that of the algal cell. Figure S8C and D show the solution SAXS curves and the repeat lamellar distances of those isolated biomembranes.

Although samples from different organisms exhibit different scattering curves, they all share typical correlation distances between 26 and 42 nm that can be assigned to the lamellar repeat distances that the charged and rigid biomembranes form. Clearly the conditions *in vivo*, with the isolated membranes and with our synthetic lipids are considerably different. Nevertheless, the repeat distances vary slightly, but still fall within a similar typical range of correlation distances (few tens of nanometers). This resemblance suggests that the range of concentrations at which our synthetic lipids deviated markedly from the behavior of typical like-charged solids is relevant to typical settings of living cells.

## References

- (1) <http://www.avantilipids.com/>.
- (2) Israelachvili, J. N. *Intermolecular and Surfaces Forces*; Second ed.; Academic Press Limited: London, 1992.
- (3) Lewis, R.; McElhaney, R. *BIOPHYSICAL JOURNAL* **2000**, *79*, 2043.
- (4) Cinelli, S.; Onori, G.; Zuzzi, S.; Bordi, F.; Cametti, C.; Sennato, S.; Bordi, F.; Cametti, C.; Sennato, S.; Diociaiuti, M. *J. Phys. Chem. B* **2007**, *111*, 10032.
- (5) Petrache, H. I.; Tristram-Nagle, S.; Gawrisch, K.; Harries, D.; Parsegian, V. A.; Nagle, J. F. *Biophysical Journal* **2004**, *86*, 1574.
- (6) Koltover, I.; Salditt, T.; Raedler, J.; Lin, A.; Slack, N.; Safinya, C. *Biophysical Journal* **1997**, *72*, TH441.
- (7) Caminiti, R.; Caracciolo, G.; Pisani, M. *Applied Physics Letters* **2005**, *86*, 3.
- (8) Rawicz, W.; Olbrich, K. C.; McIntosh, T.; Needham, D.; Evans, E. *Biophysical Journal* **2000**, *79*, 328.
- (9) Hollinshead, C. M.; Harvey, R. D.; Barlow, D. J.; Webster, J. R. P.; Hughes, A. V.; Weston, A.; Lawrence, M. J. *Langmuir* **2009**, *25*, 4070.
- (10) Kucerka, N.; Liu, Y. F.; Chu, N. J.; Petrache, H. I.; Tristram-Nagle, S. T.; Nagle, J. F. *BIOPHYSICAL JOURNAL* **2005**, *88*, 2626.
- (11) Tanford, C. *Journal of Physical Chemistry* **1972**, *76*, 3020.
- (12) David, A. In *Soft Condensed Matter Physics in Molecular and Cell Biology*; Taylor & Francis: 2006, p 97.
- (13) Pincus, P. A.; Safran, S. A. *Europhysics Letters* **1998**, *42*, 103.
- (14) Szekely, O.; Steiner, A.; Szekely, P.; Amit, E.; Asor, R.; Tamburu, C.; Raviv, U. *Langmuir* **2011**, *27*, 7419.
- (15) Ohshima, H.; Mitsui, T. *J. Colloid Interface Sci.* **1978**, *63*, 525.
- (16) Ohshima, H.; Inoko, Y.; Mitsui, T. *J. Colloid Interface Sci.* **1982**, *86*, 57.
- (17) McManus, J. J.; Radler, J. O.; Dawson, K. A. *J. Phys. Chem. B* **2003**, *107*, 9869.
- (18) Lis, L. J.; Parsegian, V. A.; Rand, R. P. *Biochemistry* **1981**, *20*, 1761.
- (19) Palade, G. E. *Proceedings of the National Academy of Sciences* **1964**, *52*, 613.

(20) Sambrook, J.; Fritsch, E. F.; Maniatis, T. *Molecular Cloning: A Laboratory Manual* 2nd ed.; Cold Spring Harbor Laboratory Press, 1989.

(21) *Guide to Yeast Genetics and Molecular Biology*; Fink, G. R.; Guthrie, C., Eds.; Academic Press: San Diego, 1991; Vol. 194.

(22) Skolnick, S.; Yeala, S. B.; Keren, N. *Biochim. Biophys. Acta-Bioenerg.* **2007**, *1767*, 814.

(23) Gorman, D. S.; Levine, R. P. *Proceedings of the National Academy of Sciences* **1965**, *54*, 1665.

(24) Andersson, B.; Akerlund, H. E.; Albertsson, P. A. *Biochimica Et Biophysica Acta* **1976**, *423*, 122.